Inorg. Chem. **2004**, *43*, 1359–1369

Structural Characterization, Magnetic Properties, and Electrospray Mass Spectrometry of Two Jahn–Teller Isomers of the Single-Molecule Magnet $[Mn_{12}O_{12}(CF_3COO)_{16}(H_2O)_4]$

Hanhua Zhao, Curtis P. Berlinguette, John Bacsa, Andrey V. Prosvirin, Jitendra K. Bera, Shane E. Tichy, Eric J. Schelter, and Kim R. Dunbar*

Department of Chemistry, Texas A&M University, P.O. Box 30012, College Station, Texas 77842-3012

Received April 29, 2003

The syntheses and characterization of two new, highly soluble, single-molecule magnets $[Mn_{12}O_{12}(CF_3COO)_{16}(H_2O)_4]\cdot 2CF_3COOH\cdot 4H_2O$ (**1**) and $[Mn_{12}O_{12}(CF_3COO)_{16}(H_2O)_4]\cdot CF_3COOH\cdot 7H_2O$ (**2**) are reported. Compound **1** was isolated from the reaction of $[Mn_{12}O_{12}(CH_3COO)_{16}(H_2O)_4]$ with trifluoroacetic acid in CH_2Cl_2. Compound **1** crystallizes in the tetragonal space group $I\bar{4}$ (No. 82) with unit cell parameters $a = b = 18.128(3)$ Å, $c = 13.048(3)$ Å, $V = 4287.9(19)$ Å^3, $Z = 2$ and is isostructural to $[Mn_{12}O_{12}(CH_3COO)_{16}(H_2O)_4]$. Compound **2** was prepared from the reaction of $[Mn_{12}O_{12}(CH_3COO)_{16}(H_2O)_4]$ with neat trifluoroacetic acid, and crystallizes in the monoclinic space group $P2_1/n$ (No. 14) with unit cell parameters $a = 15.221(8)$ Å, $b = 21.870(12)$ Å, $c = 27.217(15)$ Å, $\beta = 90.53(1)°$, $V = 9060(9)$ Å^3, and $Z = 4$. The dc magnetic susceptibility measurements in the 2–300 K temperature range support a high-spin ground state. The magnetization data collected in the 1–7 T field range from 1.8 to 4.0 K were best fit to the parameters $S = 10$, $g = 2.15$, $D = -0.65$ cm^{-1}, and $E = 0$ cm^{-1} for **1** and $S = 10$, $g = 1.87$, $D = -0.34$ cm^{-1}, and $E = -0.10$ cm^{-1} for **2**. The ac susceptibility data for compound **1** reveal out-of-phase (χ_m'') signals in the 4–7 K temperature range, whereas the χ_m'' signals for compound **2** appear below temperatures of 4 K. This variation in blocking temperatures is a consequence of the two different crystallographic forms of compounds **1** and **2**. Compound **1** exhibits the same structural geometry and distortions found in $[Mn_{12}O_{12}(CH_3COO)_{16}(H_2O)_4]$, while compound **2** is of lower molecular symmetry with two Jahn–Teller axes of distortion being oriented along oxide ligands. This different structural arrangement facilitates a different tunneling pathway that leads to a lower effective barrier for magnetization reorientation for compound **2**. The substitution of the acetate ligands by trifluoroacetic acid was monitored by mass spectrometry, which is a convenient tool for judging completion of the substitution process.

Introduction

Single-molecule magnets (SMMs) have garnered much attention over the past decade for their potential applications in high-density magnetic storage media.[1−3] In contrast to traditional magnets, which are characterized by the bulk ordering of spins within a 3D solid, SMM behavior arises from the intrinsic magnetic properties of individual molecules that leads to behavior reminiscent of superparamagnets. The hysteresis displayed by these molecules is typical of mesoscopic particles and represents the ultimate lower size limit in the quest for nanomagnetic materials. Moreover, the observation of steps in the magnetic hysteresis loops[4,5] serves as experimental evidence for quantum tunneling,[3] a finding that has implications in quantum computing applications.[6]

The presence of an appreciable thermal barrier (U) for reversing the magnetization direction of these molecules is related to the combination of a large total spin ground state

* To whom correspondence should be addressed. E-mail: dunbar@mail.chem.tamu.edu. Phone: (979) 845-5235. Fax: (979) 845-7177.

(1) Christou, G.; Gatteschi, D.; Hendrickson, D. N.; Sessoli, R. *MRS Bull.* **2000**, *25*, 66−71.
(2) Awschalom, D. D.; DiVincenzo, D. P. *Phys. Today* **1995**, *48*, 43−48.
(3) Gatteschi, D.; Sessoli, R. *Angew. Chem., Int. Ed.* **2003**, *42*, 268−297.
(4) Friedman, J.; Sarachik, M. P.; Tejada, J.; Ziolo, R. *Phys. Rev. Lett.* **1996**, *76*, 3830−3833.
(5) Thomas, L.; Lionti, F.; Ballou, R.; Gatteschi, D.; Sessoli, R.; Barbara, B. *Nature* **1996**, *383*, 145−147.
(6) Loss, D.; Divincenzo, D. P.; Grinstein, G.; Awschalom, D. D.; Smyth, J. F. *Physica B* **1993**, *189*, 189−203.

10.1021/ic030144p CCC: $27.50
Published on Web 01/22/2004

(S) and a negative uniaxial anisotropy (D). The existence of this phenomenon was first noted in the high-spin oxide-bridged cluster $[Mn_{12}O_{12}(CH_3COO)_{16}(H_2O)_4]$ (Mn_{12}-acetate),[7−9] which exhibits an $S = 10$ ground state. Since this discovery, a number of oxide-bridged clusters containing V,[10] Mn,[11−13] Fe,[14,15] Co,[16] and Ni[17] have also been shown to display SMM behavior. Despite the numerous reports in the recent literature of clusters containing a large number of paramagnetic metal centers, the most extensively studied single-molecule magnets remain the Mn_{12} family of compounds of general formula $[Mn_{12}O_{12}(CR_3COO)(H_2O)_x]^{n-}$.[18−27]

An important prerequisite for this class of compounds to be viable for applications in magnetic storage devices rests in their ability to be processed into reproducible thin films of uniform distribution of molecules.[28] Unfortunately, the fabrication of Mn_{12} thin films by conventional deposition techniques has been hampered due to the decomposition of the molecule at temperatures above 460 K.[29] Obviously "softer" methods are required if one is to successfully attach these molecules to a surface. In considering candidates for this chemistry, we selected the trifluoroacetate ligand, which has found numerous applications in dinuclear paddlewheel-type compounds.[30−32] The $[CF_3CO_2]^-$ ligand is well-known to render compounds highly soluble as well as more volatile than its $[CH_3CO_2]^-$ counterparts. Given these attributes, it is likely that trifluroacetate-based SMM's will be better candidates for incorporation into films than the corresponding acetate derivative.

Herein, we report the successful substitution of all the acetate ligands of Mn_{12}-acetate with the trifluoroacetate ligand. Two different synthetic approaches were employed to isolate two different Jahn−Teller isomeric forms of the product, namely $[Mn_{12}O_{12}(CF_3COO)_{16}(H_2O)_4]\cdot 2CF_3COOH\cdot 4H_2O$ (**1**) and $[Mn_{12}O_{12}(CF_3COO)_{16}(H_2O)_4]\cdot CF_3COOH\cdot 7H_2O$ (**2**). A thorough magneto−structural investigation revealed that both are single-molecule magnets that exhibit different blocking temperatures, a fact that is attributed to the different orientations of Jahn−Teller axes within the outer ring of Mn^{III} ions.[33] Electrospray ionization mass spectrometry (ESI-MS) was used to monitor the progress of the exchange reactions of $[Mn_{12}O_{12}(CH_3COO)_{16}(H_2O)_4]$ with trifluoroacetic acid. Earlier reports of the characterization of Mn_{12}-acetate by mass spectrometry revealed that this is an effective tool for characterizing large metal clusters.[34,35]

Experimental Section

Starting Materials. All chemicals and solvents were used as received. The starting material $[Mn_{12}O_{12}(CH_3COO)_{16}(H_2O)_4]\cdot 2CH_3COOH\cdot 4H_2O$ (Mn_{12}-acetate) was prepared according to the literature procedure.[7]

Physical Measurements. IR spectra were measured as Nujol mulls between KBr plates on a Nicolet 740 FT-IR spectrometer. Magnetic susceptibility and magnetization measurements were carried out with a Quantum Design SQUID magnetometer MPMS-XL. Samples were frozen in a gelatin capsule (Quantum Design) with eicosane. Dc magnetic measurements were performed with an applied field of 1000 G in the 2−300 K temperature range. Ac magnetic susceptibility measurements were performed in a 3 G ac field in an operating frequency range of 1−1000 Hz. Magnetization data were collected in the 0−7 T range starting at zero field at 2 K. The data were corrected for the diamagnetic contributions calculated from the Pascal constants.[36] Electrospray mass spectra were acquired using a PE Sciex (Concord, Ontario, Canada) API Qstar Pulsar using an Ionwerks time-to-digital converter, TDCx4,

(7) Lis, T. *Acta Crystallogr., Sect. B: Struct. Sci.* **1980**, *B36*, 2042−2046.
(8) Sessoli, R.; Tsai, H. L.; Schake, A. R.; Wang, S.; Vincent, J. B.; Folting, K.; Gatteschi, D.; Christou, G.; Hendrickson, D. N. *J. Am. Chem. Soc.* **1993**, *115*, 1804−1816.
(9) Sessoli, R.; Gatteschi, D.; Caneschi, A.; Novak, M. A. *Nature* **1993**, *365*, 141−143.
(10) Castro, S. L.; Sun, Z.; Grant, C. M.; Bollinger, J. C.; Hendrickson, D. N.; Christou, G. *J. Am. Chem. Soc.* **1998**, *120*, 2365−2375.
(11) Brechin, E. K.; Boskovic, C.; Wernsdorfer, W.; Yoo, J.; Yamaguchi, A.; Sanudo, E. C.; Concolino, T. R.; Rheingold, A. L.; Ishimoto, H.; Hendrickson, D. N.; Christou, G. *J. Am. Chem. Soc.* **2002**, *124*, 9710−9711.
(12) Wernsdorfer, W.; Allaga-Alcalde, N.; Hendrickson, D. N.; Christou, G. *Nature* **2002**, *416*, 406−409.
(13) Brechin, E. K.; Soler, M.; Davidson, J.; Hendrickson, D. N.; Parsons, S.; Christou, G. *Chem. Commun.* **2002**, 2252−2253.
(14) Barra, A. L.; Debrunner, P.; Gatteschi, D.; Schulz, C.; Sessoli, R. *Europhys. Lett.* **1996**, *35*, 133−138.
(15) Goodwin, J. C.; Sessoli, R.; Gatteschi, D.; Wernsdorfer, W.; Powell, A. K.; Heath, S. L.; Barra, A. L. *J. Chem. Soc., Dalton Trans.* **2000**, 4702.
(16) Yang, E. C.; Hendrickson, D. N.; Wernsdorfer, W.; Nakano, M.; Zakharov, L. N.; Sommer, R. D.; Rheingold, A. L.; Ledezma-Gairaud, M.; Christou, G. *J. Appl. Phys.* **2002**, *91*, 7382−7384.
(17) Ochsenbein, S. T.; Murrie, M.; Rusanov, E.; Stoeckli-Evans, H.; Sekine, C.; Güdel, H. U. *Inorg. Chem.* **2002**, *41*, 5133−5140.
(18) Boyd, P. D. W.; Li, Q. Y.; Vincent, J. B.; Folting, K.; Chang, H. R.; Streib, W. E.; Huffman, J. C.; Christou, G.; Hendrickson, D. N. *J. Am. Chem. Soc.* **1988**, *110*, 8537−8539.
(19) Ruiz-Molina, D.; Gerbier, P.; Rumberger, E.; Amabilino, D. B.; Guzei, I. A.; Folting, K.; Huffman, J. C.; Rheingold, A.; Christou, G.; Veciana, J.; Hendrickson, D. N. *J. Mater. Chem.* **2002**, *12*, 1152−1161.
(20) Aubin, S. M. J.; Sun, Z.; Pardi, L.; Krzystek, J.; Folting, K.; Brunel, L. C.; Rheingold, A. L.; Christou, G.; Hendrickson, D. N. *Inorg. Chem.* **1999**, *38*, 5329−5340.
(21) Soler, M.; Chandra, S. K.; Davidson, E. R.; Christou, G.; Ruiz, D.; Hendrickson, D. N. *Chem. Commun.* **2000**, 2417−2418.
(22) Kuroda-Sowa, T.; Lam, M.; Rheingold, A. L.; Frommen, C.; Reiff, W. M.; Nakano, M.; Yoo, J.; Maniero, A. L.; Brunel, L. C.; Christou, G.; Hendrickson, D. N. *Inorg. Chem.* **2001**, *40*, 6469−6480.
(23) Eppley, H. J.; Tsai, H. L.; de Vries, N.; Folting, K.; Christou, G.; Hendrickson, D. N. *J. Am. Chem. Soc.* **1995**, *117*, 301−317.
(24) Sun, Z.; Ruiz, D.; Rumberger, E.; Incarvito, C. D.; Folting, K.; Rheingold, A. L.; Christou, G.; Hendrickson, D. N. *Inorg. Chem.* **1998**, *37*, 4758−4759.
(25) Sun, Z.; Ruiz, D.; Hendrickson, D. N.; Dilley, N. R.; Maple, M. B.; Soler, M.; Folting, K.; Christou, G.; Ribas, J. *Chem. Commun.* **1999**, 1973−1974.
(26) Aubin, S. M. J.; Sun, Z.; Eppley, H. J.; Rumberger, E. M.; Guzei, I. A.; Folting, K.; Gantzel, P. K.; Rheingold, A. L.; Christou, G.; Hendrickson, D. N. *Inorg. Chem.* **2001**, *40*, 2127−2146.
(27) Artus, P.; Boskovic, C.; Yoo, J.; Streib, W. E.; Brunel, L. C.; Hendrickson, D. N.; Christou, G. *Inorg. Chem.* **2001**, *40*, 4199−4210.
(28) Leslie-Pelecky, D. L.; Rieke, R. D. *Chem. Mater.* **1996**, *8*, 1770−1783.
(29) Thermal decomposition behavior for $[Mn_{12}O_{12}(CH_3COO)_{16}(H_2O)_4]$ is submitted as Supporting Information.
(30) Matonic, J. H.; Chen, S. J.; Perlepes, S. P.; Dunbar, K. R.; Christou, G. *J. Am. Chem. Soc.* **1991**, *113*, 8169−8171.
(31) Crawford, C. A.; Day, E. F.; Saharan, V. P.; Folting, K.; Huffman, J. C.; Dunbar, K. R.; Christou, G. *Chem. Commun.* **1996**, 1113−1114.
(32) Crawford, C. A.; Matonic, J. H.; Huffman, J. C.; Folting, K.; Dunbar, K. R.; Christou, G. *Inorg. Chem.* **1997**, *36*, 2361−2371.
(33) Aubin, S. M. J.; Sun, Z. M.; Eppley, H. J.; Rumberger, E. M.; Guzei, I. A.; Folting, K.; Gantzel, P. K.; Rheingold, A. L.; Christou, G.; Hendrickson, D. N. *Inorg. Chem.* **2001**, *40*, 2127−2146.
(34) Coronado, E.; Feliz, M.; Forment-Aliaga, A.; Gomez-Garcia, C. J.; Llusar, R.; Romero, F. M. *Inorg. Chem.* **2001**, *40*, 6084−6085.
(35) Cornia, A.; Fabretti, A. C.; Pacchioni, M.; Zobbi, L.; Bonacchi, D.; Caneschi, A.; Gatteschi, D.; Biagi, R.; Del Pennino, U.; De Renzi, V.; Gurevich, L.; Van der Zant, H. S. J. *Angew. Chem., Int. Ed.* **2003**, *42*, 1645−1648.

for data recording at 625 ps time resolution. Acetonitrile solutions of the samples were electrosprayed, and the data were acquired in the negative-ion mode. The ion-spray (needle) voltage was held constant at −4.5 kV. The nozzle skimmer potential was set to −10 V to minimize fragmentation in that region. Time-of-flight (TOF) voltages were tuned to optimize the resolving power over the mass range observed, but the following parameters were typically used: grid +338 V; plate −360 V; mirror −960 V; liner −4000 V. Acquisition and data analysis were performed with the Analyst QS software.

Syntheses. $[Mn_{12}O_{12}(CF_3COO)_{16}(H_2O)_4]\cdot 2CF_3COOH\cdot 4H_2O$ (1). A suspension of $[Mn_{12}O_{12}(CH_3COO)_{16}(H_2O)_4]\cdot 2CH_3COOH\cdot 4H_2O$ (2.06 g, 1.0 mmol) in CH_2Cl_2 (40 mL) and CF_3COOH (10 mL) was stirred for 1 day. The solution was then filtered and transferred into an H-tube for slow diffusion with hexanes to yield brown-black, needle-shaped crystals suitable for single-crystal X-ray diffraction. These crystals were collected by filtration, washed with hexane, and dried under a stream of nitrogen. Yield: 0.87 g (30%). Anal. Calcd for $C_{36}F_{54}H_{18}O_{56}Mn_{12}$: C, 14.26; H, 0.60. Found: C, 14.38; H, 0.63. Characteristic IR data (cm^{-1}): ν(C═O), 1677 (s), 1640 (s), 1603 (s).

$[Mn_{12}O_{12}(CF_3COO)_{16}(H_2O)_4]\cdot CF_3COOH\cdot 7H_2O$ (2). A suspension of $[Mn_{12}O_{12}(CH_3COO)_{16}(H_2O)_4]\cdot 2CH_3COOH\cdot 4H_2O$ (4.12 g, 2.01 mmol) in CF_3COOH (20 mL) was stirred for 1 day and then filtered. The resulting filtrate was evaporated slowly at room temperature to yield brown-black crystals. These crystals were isolated and then treated with an additional volume of CF_3COOH (10 mL) and stirred overnight. The filtered solution was then evaporated slowly to yield a crop of brown-black crystals, which were redissolved in a 10 mL aliquot of CF_3COOH. The solution was evaporated slowly at room temperature to yield brown-black, needle-shaped, X-ray-quality single crystals that were collected by filtration, washed with hexane, and dried under vacuum. Yield: 0.78 g (26%). Elemental analyses were performed on various batches, but the results of the carbon analyses were consistently high. This is attributed to varying amounts of solvent in the samples. Characteristic IR data (cm^{-1}): ν(C═O), 1671 (s), 1640 (s).

X-ray Crystallography

General Procedures. A single-crystal X-ray data set was collected on a Bruker APEX CCD X-ray diffractometer for **1**. In the case of compound **2**, the data set was collected on a Bruker SMART 1000 CCD X-ray diffractometer equipped with graphite-monochromated Mo Kα radiation (λ = 0.71073 Å). The frames were integrated with the Bruker SAINT software package,[37] and the data were corrected for absorption using the program SADABS.[38] The structures were solved and refined using X-SEED,[39] a graphical interface to the SHELX[40] suite of programs.

A dark brown block of $[Mn_{12}O_{12}(CF_3COO)_{16}(H_2O)_4]\cdot 2CF_3COOH\cdot 4H_2O$ (**1**) (0.13 × 0.08 × 0.05 mm^3) was secured on a nylon loop with Paratone oil and placed in a cold N_2(g) stream at 110(2) K. A total of 5907 reflections was collected, and the crystal system was determined to be tetragonal, and belong to the space group $I\bar{4}$. The refinement was originally carried out with the same chirality as that reported for the isostructural Mn_{12}-acetate.[7] The absolute structure parameter,[41] however, indicated that compound **1** was the opposite enantiomer. The structure parameter of −0.02(3) confirmed that the absolute configuration assigned to **1** was correct. All non-solvent atoms were refined anisotropically. The asymmetric unit contains one-quarter of the dodecanuclear cluster and one unambiguous H_2O solvent molecule. Eight of 16 $-CF_3$ groups of the $[CF_3COO]^-$ ligands were disordered and were modeled over two positions using appropriate C−F and F−F distances (1.33 and 2.14 Å, respectively) of CF_3 groups in CF_3COOH molecules. Three relatively large residual peaks in the difference maps could not be definitively assigned. A low-temperature collection at T = 30 K was carried out, but unfortunately, these data did not help with the resolution of the disorder. These peaks were located in two voids in the unit cell, each with a volume of 270(80) $Å^3$,[42] which were large enough to accommodate two CF_3COOH molecules.[43] The molecular formula proposed for $[Mn_{12}O_{12}(CF_3COO)_{16}(H_2O)_4]\cdot 2CF_3COOH\cdot 4H_2O$ is supported by elemental analysis. The final refinement was based on 4281 reflections with $F_o > 4\sigma(F_o)$ and 358 parameters ($R1$ = 0.0530, $wR2$ = 0.1199). The maximum and minimum peaks in the final difference Fourier map corresponded to 0.61 and −0.55 e/$Å^3$, respectively, with a goodness-of-fit value of 1.025.

A dark brown needle of $[Mn_{12}O_{12}(CF_3COO)_{16}(H_2O)_4]\cdot CF_3COOH\cdot 7H_2O$ (**2**) (0.35 × 0.18 × 0.06 mm^3) was secured on a nylon loop with paratone oil and placed in a cold N_2(g) stream at 110(2) K. A total of 44546 reflections were collected. Preliminary indexing indicated that the unit cell was either orthorhombic or monoclinic with $\beta \sim 90°$, an observation that typically indicates the presence of pseudo-merohedral twinning. An investigation of the diffraction patterns indicated that the crystal belongs to the monoclinic crystal system with systematic absences that are in accord with the space group $P2_1/n$. The application of various twin laws led to the selection of a 2-fold rotation about the *a*-axis as the best solution and resulted in the reduction of $R1$ from 0.27 to 0.11. The refinement in the orthorhombic cell did not lead to a satisfactory structure solution. The molecule is situated on a general position, and the asymmetric unit contains an entire $[Mn_{12}O_{12}(CF_3COO)_{16}(H_2O)_4]$ molecule. All metal ions were refined anisotropically. Eleven of the 16 $-CF_3$ groups of the CF_3COOH ligands were disordered and were modeled over two positions using appropriate C−F and F−F distances. The residual electron density obtained after refinement of the cluster was diffuse but was successfully assigned to two disordered CF_3COOH molecules. These disordered CF_3COOH molecules, which required the appropriate constraints, were each located on inversion centers. Residual electron density was used to assign atoms belonging to a second component at 50% occupancy. The thermal parameters of atoms in both components were restrained to be equal. The remaining peaks were assigned as O atoms with fractional site occupancy until the maximum and minimum peaks in the final difference Fourier map corresponded to 1.18 and −1.07 e/$Å^3$, respectively, with a goodness-of-fit value of 1.028. The final refinement cycle was based on 4283 reflections with $F_o > 4\sigma(F_o)$ and 858 parameters ($R1$ = 0.1053, $wR2$ = 0.2423).

Crystal parameters and basic information pertaining to data collection and refinement for both structures are summarized in Table 1. Relevant bonding distances and angles are listed in Tables 2−5.

(36) Boudreaux, E. A.; Mulay, L. N. *Theory and Applications of Molecular Paramagnetism*; 1976; p 512.
(37) *Saint, Program for area detector absorption correction*; Siemens Analytical X-ray Instruments: 1994.
(38) *SADABS*; Bruker AXS, Inc.: Madison, WI, 2001.
(39) Barbour, L. J. *J. Supramol. Chem.* **2003**, *1*, 189−191.
(40) Sheldrick, G. *Shelxl-97 Program for Crystal Structure Refinement*; University of Gottingen: Gottingen, Germany, 1997.
(41) Flack, H. D. *Acta Crystallogr., Sect. A* **1983**, *39*, 876−881.
(42) Spek, A. L. *J. Appl. Crystallogr.* **2003**, *36*, 7−13.
(43) Allinger, N. L.; Yuh, Y. H.; Lii, J. H. *J. Am. Chem. Soc.* **1989**, *111*, 8551−8566.

Table 1. Crystallographic Data and Structural Refinement Parameters for Compounds $[Mn_{12}O_{12}(CF_3COO)_{16}(H_2O)_4]\cdot 2CF_3COOH\cdot 4H_2O$ (**1**) and $[Mn_{12}O_{12}(CF_3COO)_{16}(H_2O)_4]\cdot CF_3COOH\cdot 7H_2O$ (**2**)

	1	**2**
chem formula	$C_{32}H_{28}F_{48}Mn_{12}O_{58}$	$C_{34}H_{23}F_{51}Mn_{12}O_{57}$
a (Å)	18.128(5)	15.221(8)
b (Å)	18.128(5)	21.870(12)
c (Å)	13.048(3)	27.217(15)
α (deg)	90	90
β (deg)	90	90.526(10)
γ (deg)	90	90
V (Å^3)	4287.9(19)	9060(9)
Z	2	4
fw	2911.7	2971.7
space group	$I\bar{4}$	$P2_1/n$
T (K)	110(2)	110(2)
λ (Å)	0.71073	0.71073
D_{calcd} (g cm^{-3})	2.233	2.162
μ (cm^{-1})	1.911	1.815
*R*1 ($I > 2\sigma(I)$)[a]	0.0530	0.1053
*R*2 (all data)[b,c]	0.1199	0.2423

[a] $R1 = \sum(|F_o| - |F_c|)/\sum|F_o|$. [b] $wR2 = \{\sum w[(F_o^2 - F_c^2)^2]/\sum w(F_o^2)^2]\}^{1/2}$. [c] $w = 1/[\sigma^2(F_o^2) + (0.0904P)^2]$, where $P = (F_o^2 + 2F_c^2)/3$.

Table 2. Selected Bond Distances (Å) for Compound **1**

Mn(1)−O(1)	1.922(4)	Mn(2)−O(6)	2.231(5)
Mn(1)−O(1)′	1.931(4)	Mn(2)−O(8)	1.939(5)
Mn(1)−O(1)″	1.895(5)	Mn(2)−O(10)	1.948(5)
Mn(1)−O(2)	1.879(4)	Mn(3)−O(2)	1.891(4)
Mn(1)−O(3)	1.898(4)	Mn(3)−O(3)′	1.903(4)
Mn(1)−O(4)	1.924(4)	Mn(3)−O(7)	2.165(5)
Mn(2)−O(2)	1.897(4)	Mn(3)−O(9)	2.003(5)
Mn(2)−O(3)	1.917(4)	Mn(3)−O(11)	2.005(5)
Mn(2)−O(5)	2.234(5)	Mn(3)−O(12)	2.160(5)

Table 3. Selected Bond Angles (deg) for Compound **1**

O(2)−Mn(1)−O(3)	84.83(19)	O(8)−Mn(2)−O(5)	89.7(2)
O(2)−Mn(1)−O(1)	172.76(19)	O(10)−Mn(2)−O(5)	93.7(2)
O(3)−Mn(1)−O(1)	100.01(17)	O(6)−Mn(2)−O(5)	174.24(19)
O(2)−Mn(1)−O(4)	94.14(18)	O(2)−Mn(3)−O(9)	174.01(19)
O(3)−Mn(1)−O(4)	92.28(18)	O(2)−Mn(3)−O(11)	91.11(19)
O(1)−Mn(1)−O(4)	91.06(18)	O(9)−Mn(3)−O(11)	82.9(2)
O(2)−Mn(2)−O(3)	83.83(17)	O(2)−Mn(3)−O(12)	96.94(18)
O(2)−Mn(2)−O(8)	175.5(2)	O(9)−Mn(3)−O(12)	82.59(19)
O(3)−Mn(2)−O(8)	96.37(19)	O(11)−Mn(3)−O(12)	85.48(19)
O(2)−Mn(2)−O(10)	94.96(19)	O(2)−Mn(3)−O(7)	93.08(18)
O(3)−Mn(2)−O(10)	178.1(2)	O(9)−Mn(3)−O(7)	86.42(19)
O(8)−Mn(2)−O(10)	84.7(2)	O(11)−Mn(3)−O(7)	84.52(18)
O(2)−Mn(2)−O(6)	90.51(19)	O(12)−Mn(3)−O(7)	165.97(19)
O(3)−Mn(2)−O(6)	90.52(18)	Mn(1)−O(2)−Mn(3)	134.7(2)
O(8)−Mn(2)−O(6)	94.0(2)	Mn(1)−O(2)−Mn(2)	95.65(19)
O(10)−Mn(2)−O(6)	91.0(2)	Mn(3)−O(2)−Mn(2)	127.9(2)
O(2)−Mn(2)−O(5)	85.79(18)	Mn(1)−O(3)−Mn(2)	94.34(19)
O(3)−Mn(2)−O(5)	84.71(17)		

Results and Discussion

Syntheses. Compounds **1** and **2**, prepared by the complete substitution of acetate with trifluoroacetate, constitute two new derivatives of the Mn_{12} family of compounds. Complete substitution of acetate ligands occurs at a faster rate in an organic/acid medium than the reaction in corresponding neat acid. It was noted that prolonged reaction times in the organic/acid medium leads to a decomposition of the dodecanuclear cluster to yield the mixed-valence trinuclear species, $[Mn^{II}Mn^{III}_2O(CF_3COO)_6(OH_2)_3]$.[44] When a pure sample of compound **2** is dissolved in a CH_2Cl_2/CF_3COOH medium, however, the resulting mixture produces compound **1** upon slow diffusion with hexanes. This result clearly indicates that the presence of CH_2Cl_2 in the CF_3COOH medium results in an isomerization from **2** to **1**.

As stated earlier, the presence of the $-CF_3$ groups on the periphery of the Mn_{12} cluster is expected to enhance the solubility of the compounds, and, indeed, this is the case. Both isomers are highly soluble in acetone, THF, MeCN,

Table 4. Selected Bond Distances (Å) for Compound **2**

Mn(1)−O(1)	1.885(10)	Mn(9)−O(10)	1.909(10)
Mn(1)−O(2)	1.849(9)	Mn(9)−O(22)	1.924(10)
Mn(1)−O(3)	1.911(11)	Mn(9)−O(23)	1.975(11)
Mn(1)−O(32)	1.897(11)	Mn(9)−O(34)	2.237(11)
Mn(1)−O(5)	1.884(10)	Mn(9)−O(35)	2.176(10)
Mn(1)−O(6)	1.887(10)	Mn(9)−O(9)	1.886(10)
Mn(6)−O(28)	1.969(13)	Mn(11)−O(11)	1.872(9)
Mn(6)−O(29)	1.971(12)	Mn(11)−O(12)	1.922(10)
Mn(6)−O(45)	2.145(11)	Mn(11)−O(16)	1.973(11)
Mn(6)−O(46)	2.137(13)	Mn(11)−O(18)	2.236(9)
Mn(6)−O(6)	1.878(11)	Mn(11)−O(19)	1.930(10)
Mn(6)−O(7)	1.892(10)	Mn(11)−O(37)	2.233(10)
Mn(8)−O(24)	1.989(10)	Mn(12)−O(12)	2.036(10)
Mn(8)−O(25)	2.033(12)	Mn(12)−O(14)	2.091(12)
Mn(8)−O(36)	2.023(11)	Mn(12)−O(15)	1.963(11)
Mn(8)−O(44)	2.018(10)	Mn(12)−O(17)	1.961(10)
Mn(8)−O(8)	1.933(9)	Mn(12)−O(42)	1.957(10)
Mn(8)−O(9)	1.956(10)	Mn(12)−O(5)	1.904(10)

Table 5. Selected Bond Angles (deg) for Compound **2**

O(2)−Mn(1)−O(1)	82.9(4)	O(9)−Mn(9)−O(10)	82.4(4)
O(2)−Mn(1)−O(5)	93.4(4)	O(9)−Mn(9)−O(22)	177.1(4)
O(1)−Mn(1)−O(5)	98.7(4)	O(10)−Mn(9)−O(22)	96.2(4)
O(2)−Mn(1)−O(32)	172.8(5)	O(9)−Mn(9)−O(23)	95.7(4)
O(1)−Mn(1)−O(32)	93.6(4)	O(10)−Mn(9)−O(23)	173.8(4)
O(5)−Mn(1)−O(32)	93.4(5)	O(22)−Mn(9)−O(23)	85.4(4)
O(2)−Mn(1)−O(6)	90.6(4)	O(9)−Mn(9)−O(35)	92.4(4)
O(1)−Mn(1)−O(6)	173.4(4)	O(10)−Mn(9)−O(35)	93.9(4)
O(5)−Mn(1)−O(6)	82.1(4)	O(22)−Mn(9)−O(35)	90.1(4)
O(32)−Mn(1)−O(6)	92.9(4)	O(23)−Mn(9)−O(35)	92.1(4)
O(2)−Mn(1)−O(3)	83.7(4)	O(9)−Mn(9)−O(34)	87.2(4)
O(1)−Mn(1)−O(3)	81.3(5)	O(10)−Mn(9)−O(34)	85.0(4)
O(5)−Mn(1)−O(3)	177.0(4)	O(22)−Mn(9)−O(34)	90.2(4)
O(32)−Mn(1)−O(3)	89.6(5)	O(23)−Mn(9)−O(34)	89.0(4)
O(6)−Mn(1)−O(3)	97.5(5)	O(35)−Mn(9)−O(34)	178.8(4)
O(6)−Mn(6)−O(7)	94.7(4)	O(11)−Mn(11)−O(12)	83.4(4)
O(6)−Mn(6)−O(29)	91.6(5)	O(11)−Mn(11)−O(19)	94.9(4)
O(7)−Mn(6)−O(29)	173.0(5)	O(12)−Mn(11)−O(19)	177.0(4)
O(6)−Mn(6)−O(28)	173.8(5)	O(11)−Mn(11)−O(16)	174.4(4)
O(7)−Mn(6)−O(28)	91.4(5)	O(12)−Mn(11)−O(16)	94.2(4)
O(29)−Mn(6)−O(28)	82.4(5)	O(19)−Mn(11)−O(16)	87.3(4)
O(6)−Mn(6)−O(46)	94.4(5)	O(11)−Mn(11)−O(37)	85.4(4)
O(7)−Mn(6)−O(46)	94.3(5)	O(12)−Mn(11)−O(37)	87.8(4)
O(29)−Mn(6)−O(46)	88.3(5)	O(19)−Mn(11)−O(37)	89.7(4)
O(28)−Mn(6)−O(46)	84.1(5)	O(16)−Mn(11)−O(37)	89.4(4)
O(6)−Mn(6)−O(45)	93.1(4)	O(11)−Mn(11)−O(18)	93.9(4)
O(7)−Mn(6)−O(45)	93.9(4)	O(12)−Mn(11)−O(18)	90.4(4)
O(29)−Mn(6)−O(45)	82.7(5)	O(19)−Mn(11)−O(18)	92.2(4)
O(28)−Mn(6)−O(45)	87.5(5)	O(16)−Mn(11)−O(18)	91.2(4)
O(46)−Mn(6)−O(45)	168.4(4)	O(37)−Mn(11)−O(18)	178.1(4)
O(8)−Mn(8)−O(9)	93.2(4)	O(5)−Mn(12)−O(42)	92.9(4)
O(8)−Mn(8)−O(24)	175.4(4)	O(5)−Mn(12)−O(15)	174.7(4)
O(9)−Mn(8)−O(24)	91.1(4)	O(42)−Mn(12)−O(15)	86.4(4)
O(8)−Mn(8)−O(44)	92.9(4)	O(5)−Mn(12)−O(17)	89.5(4)
O(9)−Mn(8)−O(44)	90.0(4)	O(42)−Mn(12)−O(17)	176.1(5)
O(24)−Mn(8)−O(44)	85.4(4)	O(15)−Mn(12)−O(17)	90.9(4)
O(8)−Mn(8)−O(36)	88.9(4)	O(5)−Mn(12)−O(12)	92.7(4)
O(9)−Mn(8)−O(36)	94.0(4)	O(42)−Mn(12)−O(12)	86.2(4)
O(24)−Mn(8)−O(36)	92.5(4)	O(15)−Mn(12)−O(12)	92.5(4)
O(44)−Mn(8)−O(36)	175.5(5)	O(17)−Mn(12)−O(12)	96.8(4)
O(8)−Mn(8)−O(25)	93.1(4)	O(5)−Mn(12)−O(14)	91.3(4)
O(9)−Mn(8)−O(25)	173.4(5)	O(42)−Mn(12)−O(14)	91.4(4)
O(24)−Mn(8)−O(25)	82.7(4)	O(15)−Mn(12)−O(14)	83.5(4)
O(44)−Mn(8)−O(25)	91.8(4)	O(17)−Mn(12)−O(14)	85.5(4)
O(36)−Mn(8)−O(25)	84.0(5)	O(12)−Mn(12)−O(14)	175.4(4)

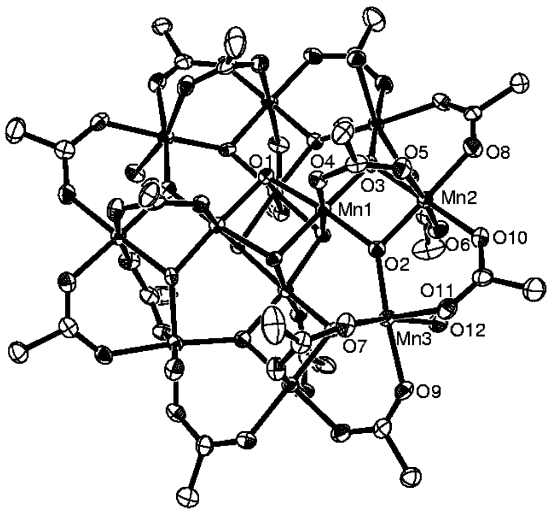

Figure 1. ORTEP representation for $[Mn_{12}O_{12}(CF_3COO)_{16}(H_2O)_4]\cdot 2CF_3COOH\cdot 4H_2O$ (**1**) drawn at the 50% probability level. (F atoms have been omitted for clarity.)

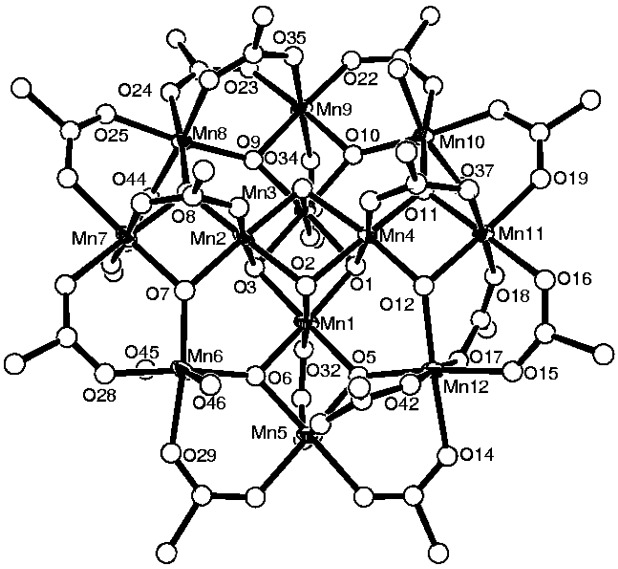

Figure 2. ORTEP representation for $[Mn_{12}O_{12}(CF_3COO)_{16}(H_2O)_4]\cdot CF_3COOH\cdot 7H_2O$ (**2**) drawn at the 50% probability level. (F atoms have been omitted for clarity.)

MeOH, EtOH, $MeNO_2$, DMF, and DMSO. Moreover, the trifluoroacetate ligands are also easily substituted by other carboxylate ligands (vida infra).

Molecular Structure of $[Mn_{12}O_{12}(CF_3COO)_{16}(H_2O)_4]\cdot 2CF_3COOH\cdot 4H_2O$ (1). Compound **1** (depicted in Figure 1) crystallizes in the space group $I\bar{4}$ and is isostructural with the original Mn_{12}-acetate complex. Not surprisingly, the unit cell volume is larger relative to the acetate analogue (4288 $Å^3$ versus 3716 $Å^3$) in accord with the larger volumes of the $-CF_3$ and $-CH_3$ groups of 37 and 29 $Å^3$, respectively.[43] The molecule is best described as a dodecanuclear $[Mn_{12}(\mu_3\text{-}O)_{12}]$ core composed of a central cubane $[Mn^{IV}{}_4O_4]^{8+}$ unit that is bridged to a peripheral ring of Mn^{III} atoms linked by O^{2-} ions. The molecule is located on the symmetry element $\bar{4}$, which gives rise to two crystallographic unique Mn^{III} atoms (Mn(2) and Mn(3)) and one Mn^{IV} atom (Mn(1)) in the asymmetric unit. The Mn centers were assigned formal charges of +3 and +4 on the basis of the Mn−O bond distances (which are typical for Mn^{III} and Mn^{IV} ions). These assignments are authenticated by the bond valence method and are the same as those reported for many other Mn_{12} complexes of this family.[45−50] The eight Mn(III) ions exhibit similar Jahn−Teller distortions perpendicular to the plane of the molecule. The Mn(1) ion is linked to the Mn(2) and Mn(3) ions via triply bridged oxygen ions and to the Mn(2) ion by a trifluoroacetate ligand. The Mn(2) and Mn(3) ions are bridged by three trifluoroacetate ions, with the coordination environment around the Mn(3) atom being completed by a water molecule. The Mn^{IV} ion adopts an octahedral geometry with bond distances that range from 1.875(4) to 1.933(4) Å. Each Jahn−Teller distorted Mn^{III} ion is characterized by a pair of long Mn−O bond distances to two trans coordinated trifluoroacetate ligands (2.231(5)/2.234(5) Å) and a pair of short Mn−O distances (1.897(5)/1.917(5) Å) (refer to Figure 4 with darker bonds to emphasize direction of the axes). The periphery of the molecule consists of 16 η^2,μ_2-triflouroacetate molecules and four H_2O ligands. The four H_2O molecules coordinated to the Mn(2) and Mn(3) atoms are oriented trans to the bridging ligand in an alternating up−down−up−down fashion that leads to $\bar{4}$ crystallographic site symmetry for the core of the molecule (Figure 3), the highest possible for the Mn_{12} family of compounds.

Molecular Structure of $[Mn_{12}O_{12}(CF_3COO)_{16}(H_2O)_4]\cdot CF_3COOH\cdot 7H_2O$ (2). As mentioned earlier, the successful isolation of pure crystals of **2** requires repeated treatments of Mn_{12}-acetate with neat trifluoroacetic acid. It is important to note that single crystals with essentially the same unit cell as that of pure crystals of **2** were obtained after one acid treatment only, but additional characterization by ESI-MS conclusively demonstrated that these crystals contain residual acetate ligands (vide infra). This provides incontrovertible evidence that multiple treatments of the product with fresh acid are required to obtain the fully substituted product, $[Mn_{12}O_{12}(CF_3COO)_{16}(H_2O)_4]\cdot CF_3COOH\cdot 7H_2O$ (**2**).

The familiar $[Mn_{12}(\mu_3\text{-}O)_{12}]$ core is also present in the clusters that crystallize in compound **2** (Figure 2), but these molecules exhibit a lower symmetry which leads to the space group $P2_1/n$. There is a pseudo-2-fold rotation axis that imposes nearly ideal C_2 symmetry, but the molecule is

(44) It is worth noting that these trinuclear species are traditionally used to prepare a variety of Mn_{12} derivatives but that the fluorinated version of the trinuclear species does not appear to be a feasible precursor for higher nuclearity clusters: Zhao, H.; Berlinguette, C. P.; Bacsa, J.; Tichy, S. E.; Dunbar, K. R. *J. Clust. Sc.* **2003**, *14*, 235−252.

(45) Aubin, S. M. J.; Sun, Z. M.; Eppley, H. J.; Rumberger, R. M.; Guzei, I. A.; Folting, K.; Gantzel, P. K.; Rheingold, A. L.; Christou, G.; Hendrickson, D. N. *Polyhedron* **2001**, *20*, 1139−1145.

(46) Kuroda-Sowa, T.; Nakano, M.; Christou, G.; Hendrickson, D. N. *Polyhedron* **2001**, *20*, 1529−1536.

(47) Sun, Z. M.; Ruiz, D.; Rumberger, E.; Incarvito, C. D.; Folting, K.; Rheingold, A. L.; Christou, G.; Hendrickson, D. N. *Inorg. Chem.* **1998**, *37*, 4758−4759.

(48) An, J.; Chen, Z. D.; Bian, J.; Chen, J. T.; Wang, S. X.; Gao, S.; Xu, G. X. *Inorg. Chim. Acta* **2000**, *299*, 28−34.

(49) Brown, I. D.; Wu, K. K. *Acta Crystallogr., Sect. B: Struct. Sci.* **1976**, *32*, 1957−1959.

(50) The oxidation state assignment for each of the Mn ions using the bond valence method is submitted as Supporting Information.

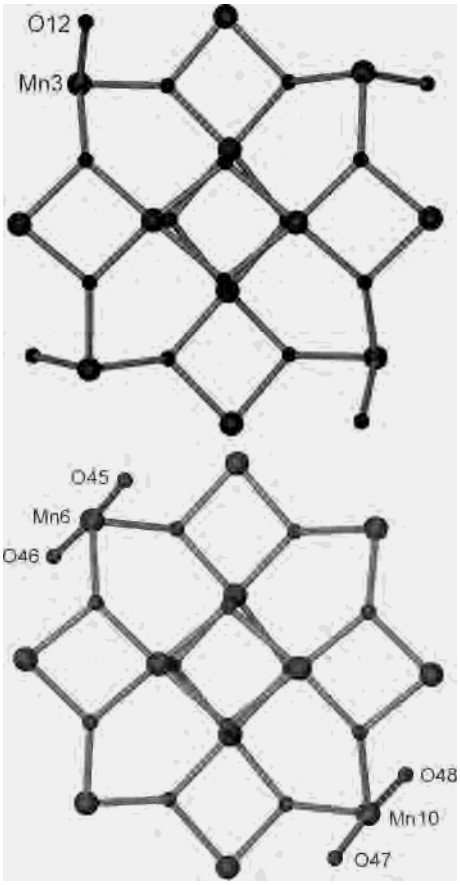

Figure 3. Structural core of compounds **1** (top) and **2** (bottom) illustrating the different coordination positions of the four H_2O molecules.

situated on a general position; the result is 12 crystallographically independent Mn atoms. The Mn(1)−Mn(4) atoms comprise the $[Mn^{IV}{}_4O_4]^{8+}$ cubane core and are further linked to the outer ring of eight Mn atoms, labeled Mn(5)−Mn(12), by μ_3-O^{2-} and η^2,μ_2-triflouroacetate ligands. The local connectivity of the cubane core displays bond distances and angles similar to those in compound **1**, with a similar, but not identical, arrangement of trifluoroacetate molecules in the peripheral ring. The trifluoroacetate groups that bridge the cubane core to the outer ring of eight Mn atoms are in the same up−down−up−down arrangement (i.e. pseudo-S_4 site symmetry) as observed for compound **1**, but there are key differences in the geometries and metrical parameters. One distinct feature is that the four water molecules in **2** are coordinated to only two metal atoms; these are trans to each other and are bound to the Mn(6) and the Mn(10) ions (Figure 3).[33,51,52] This type of coordination is in contrast to compound **1**, where four molecules are distributed over four Mn^{III} centers, and previously reported JT isomers.[33] The Mn(6) and Mn(10) atoms are bound to their respective neighbors by only two bridging trifluoroacetate ligands, respectively. The Mn(7) and Mn(11) atoms are connected to neighboring Mn centers in the ring by three bridging trifluoroacetate ligands and to the cubane core by a μ_3-O^{2-} and a bridging trifluoroacetate ligand. The Mn(5) and Mn(9) atoms are each coordinated to four bridging trifluoroacetate ligands, one of which is connected to the central core. The Mn(8) and Mn(12) atoms are also coordinated to four bridging trifluoroacetate groups that serve to bridge to other Mn atoms in the outer ring and two μ_3-O^{2-} groups that provide the only connectivity to the core for these Mn centers.

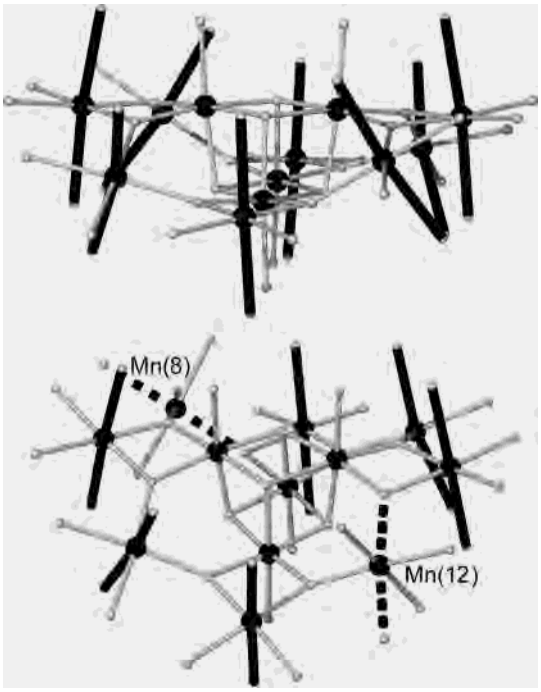

Figure 4. Schematic representation of compounds **1** (top) and **2** (bottom) emphasizing the orientation of the elongated Jahn−Teller axes. The broken line for compound **2** depicts the long JT axis of distortion that is directed at the μ_3-O^{2-}.

The Mn atoms that constitute the cubane core all exhibit Mn−O bond distances (1.849(9)−1.970(9) Å) comparable to those of the cubane core in compound **1**. Notably, the bond distances and geometries for the eight peripheral Mn^{III} atoms in the outer ring are not analogous to those of compound **1**. The Mn(6) and Mn(10) atoms that are coordinated to the water molecules exhibit well-defined elongated JT axes of distortion (2.15(1)/2.14(1) Å) perpendicular to the plane. The same well-defined JT distortion and directionality are also observed for the Mn(5), Mn(7), Mn(9), and Mn(11) ions; the elongated axes directed toward the O atoms of the bridging trifluoroacetate ligands. On the contrary, the Mn(8)−O bonds are much less obvious in terms of the principal JT axis, with values that range from 1.94(9) to 2.03(2) Å.[53] In the case of the Mn(12) center, however, there is clearly an elongated JT axis (2.036(9) Å) pointed directly at an oxide ligand (Figure 4), a feature that was also noted for previous examples of Mn_{12} isomers.[25,33,45,47] This result is surprising, as the elongated JT distortions tend to occur along the weaker bonds, in this case, the $Mn-O_2CCF_3$

(51) Boyd, P. D. W.; Li, Q.; Vincent, J. B.; Folting, K.; Chang, H. R.; Streib, W. E.; Huffman, J. C.; Christou, G.; Hendrickson, D. N. *J. Am. Chem. Soc.* **1988**, *110*, 8537−8539.

(52) Takeda, K.; Awaga, K.; Inabe, T. *Phys. Rev. B: Condens. Matter* **1998**, *57*, R11062−R11064.

(53) The oxidation state assignment of the Mn(8) ion is supported by the Mn−O bond distances, which are too short for Mn^{II} and are comparable to Mn^{III}−O distances in related structures. This was confirmed by bond valence calculations (submitted as Supporting Information).

rather than O^{2-} ion. A consequence of this unusual type of distortion is that the JT axis about the Mn(12) atom and, to a lesser extent, the Mn(8) atom is oriented more along the pseudoequatorial plane rather than the axial direction of the molecule. This is an important issue because the orientation of the JT axes (Figure 4) figure prominently in the overall axial anisotropy (*D*) of these "Jahn−Teller isomers", and therefore variations in the magnetic behavior are expected.[25,33,45,47]

Electrospray Mass Spectrometry. Traditional solid-state characterization methods are unable to provide definitive evidence for complete substitution of the acetate ligands by trifluoroacetate groups in bulk samples of these reactions. Single-crystal X-ray diffraction studies on individual crystals also do not rule out the possibility of a small residual amount of acetate ligands, as disorder would effectively prevent discerning between 100% occupancy of trifluoroacetate and cases where the impurity of acetate was low. In such situations, ESI-MS is an attractive analytical tool to examine the presence of such impurities. A relatively soft ionization technique that leads to minimal fragmentation during the ionization process, ESI-MS can be coupled to a time-of-flight mass spectrometer (TOF MS) to obtain a high degree of mass accuracy (<5 ppm) and ultrahigh resolution (>10 000).[54] An increasing number of applications of this powerful technique in the field of inorganic molecules are appearing in the literature,[55] and, in fact, the technique has been cited as being useful for characterizing samples of $[Mn_{12}O_{12}(CRCOO)_{16}(H_2O)_4]$ for which single crystals cannot be obtained.[19,34,35] In this study, we describe the application of ESI-MS for examining the progress of exchange reactions of Mn_{12}-acetate with the triflouroacetate ligand.

To assess the stability of the Mn_{12} core under the conditions used for these experiments, a mass spectrum of the parent Mn_{12}-acetate compound was first recorded.[56] The highest intensity signal corresponded to $[Mn_{12}O_{12}(CH_3COO)_{16}]^-$ at *m*/*z* 1795, which is consistent with the reported spectrum for this complex.[19] A series of relatively low-abundance peaks (<10% compared to the molecular ion peak) decreasing by 59 atomic mass units were also observed. These signals are attributed to the stepwise loss of $[CH_3CO_2]^-$ units by in-source fragmentation.

Corresponding ESI-MS data for the Mn_{12}-trifluroacetate clusters, **1** and **2**, proved to be more difficult to obtain. Considerable effort was expended to optimize the solvent medium (e.g. various combinations of MeOH, EtOH, CH_2Cl_2, $CHCl_3$, and MeCN) and analyte concentration. The best results were obtained for analyte concentrations of $\sim 10\ \mu$M in MeCN, which produced an appreciably intense parent ion peak in the negative ion mode for both **1** and **2**. The positive ion mode was found to lead to much more complicated mass spectra, so it was not used any further in these studies. To examine whether alcohols cause decomposition of the clusters, a sample of $[Mn_{12}O_{12}(CF_3COO)_{16}(H_2O)_4]$ (**1**) was dissolved in MeOH and maintained at room temperature for 1 h. The methanol was then removed under vacuum, and **1** was redissolved in acetonitrile. The mass spectrum of **1** after this treatment was comparable to that of the original crystalline complex dissolved in MeCN; therefore, it appears that the cluster is stable in methanol. This also suggests that it is necessary to use MeCN as the solvent for the ESI-MS studies as MeOH is a poor solvent for these experiments.

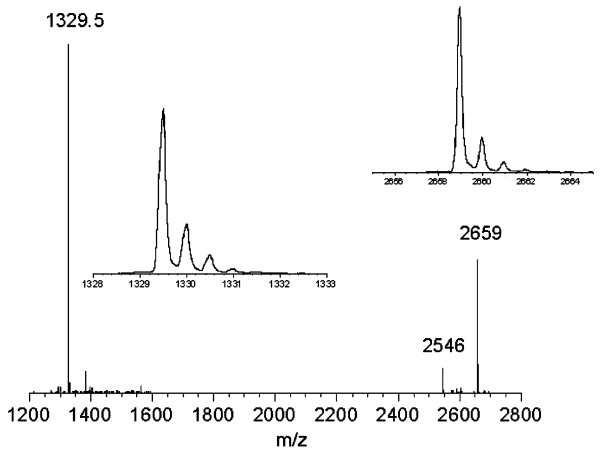

Figure 5. ESI-MS data for a CH_3CN solution of $[Mn_{12}O_{12}(CF_3COO)_{16}(H_2O)_4]\cdot 2CF_3COOH\cdot 4H_2O$ (**1**) recorded in the negative-ion mode. Inset: Regions at *m*/*z* 1329.5 and 2659 expanded for clarity.

The ESI-MS spectrum in the negative-ion mode for **1** dissolved in MeCN is depicted in Figure 5. The highest mass signal at *m*/*z* 2659 in the mass spectrum is assigned to the $[Mn_{12}O_{12}(CF_3COO)_{16}]^-$ cluster. Unlike the Mn_{12}-acetate complex, the corresponding doubly charged species $[Mn_{12}O_{12}(CF_3COO)_{16}]^{2-}$ at *m*/*z* 1329.5 is the most dominant signal in the mass spectrum of **1**. Loss of $[CF_3COO]^-$ (*m*/*z* 113) due to in-source fragmentation was also observed. An identical mass spectrum was obtained for complex **2** under similar experimental conditions.[57]

The mass spectra of the isolated complexes confirm the complete replacement of all of the bridging acetates by triflouroacetate in the final products and further support the conclusion that the Mn_{12} core is relatively stable in the trifluoroacetate derivatives. Samples recovered at intermediate stages of the reaction show the presence of partially substituted clusters with a combination of $[CF_3CO_2]^-$:$[CH_3CO_2]^-$ ligands in the ratio of 16:0 through 11:5 (Figure 6). The reaction conditions were modified on the basis of these observations until the fully substituted product (Figure 5) was obtained in a pure form.

Reactivity Studies of Compound 1 Monitored by ESI-MS. Electrospray mass spectrometry was used to monitor the treatment of complex **1** with a variety of acids, namely, CH_3CO_2H, $C_6H_5CO_2H$, $(CH_3)CCH_2CO_2H$, $NC_5H_4CO_2H$, and HNO_3. In a typical reaction, a quantity of **1** (0.050 g) was dissolved in CH_3CN (10 mL), treated with the appropriate acid, and stirred for 20 h at 30 °C. Aliquots of the solutions were diluted with CH_3CN and injected into the mass

(54) Koomen, J. M.; Russell, W. K.; Tichy, S. E.; Russell, D. H. *J. Mass Spectrom.* **2002**, *37*, 357−371.
(55) Schalley, C. A.; Muller, T.; Linnartz, P.; Witt, M.; Schafer, M.; Lutzen, A. *Chem.−Eur. J.* **2002**, *8*, 3538−3551.
(56) The ESI-MS spectra for $[MnO_{12}(CF_3COO)_{16}(OH_2)_4]$ are submitted as Supporting Information.
(57) The ESI-MS spectra for compound **2** are submitted as Supporting Information.

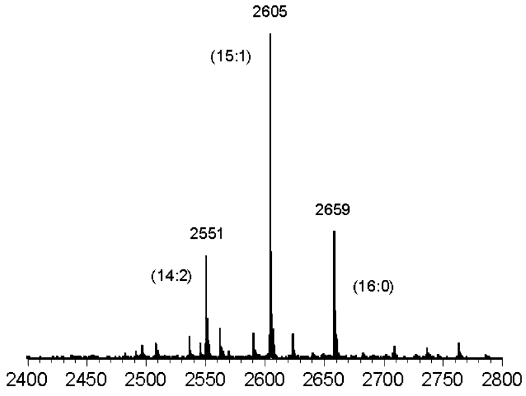

Figure 6. ESI-MS data of a sample demonstrating the incomplete replacement of the acetate by trifluoroacetate.

Table 6. Reactivity Studies for $[Mn_{12}O_{12}(CF_3COO)_{16}(H_2O)_4]\cdot 2CF_3COOH\cdot 4H_2O$ (**1**) Monitored by ESI-MS

	$[Mn_{12}O_{12}(CF_3COO)_x(acid)_{16-x}]$
acid	x
acetic acid	3−13
^{t}Bu-acetic acid	4−10
nitric acid	no assignable peaks
isonicotinic acid	9−15

spectrometer. A summary of the reactivity study is depicted in Table 6.[58]

ESI-MS data on the solution obtained by the treatment of **1** with 5 drops of glacial acetic acid revealed the presence of a mixed-ligand trifluoroacetate−acetate species, $[Mn_{12}O_{12}(CF_3COO)_x(CH_3COO)_{16-x}]$, in which x varies from 3 to 13. The spectrum includes a series of peaks separated by 54 and 27 atomic mass units (in the singly and doubly charged regions, respectively) that are assigned as substitution products of trifluoroacetate with acetate ligands. It is noted that complete substitution was not achieved under the experimental conditions mentioned above. The treatment of **1** with $(CH_3)_3CCH_2CO_2H$ led to similar results, namely, the presence of partially substituted complexes with trifluoroacetate/*tert*-butylacetate ratios varying from 10:6 to 4:12.

The treatment of a MeCN solution of **1** with 5 drops of 0.226 M HNO_3 in CH_3CN produced a dark brown reaction solution after 20 h of stirring. The ESI-MS data revealed numerous doubly charged species of molecular weights between m/z 1600 and 2400. The random nature and number of peaks suggests decomposition of the complex, and no practical assignment of any $[Mn_{12}O_{12}(CF_3COO)_x(NO_3)_{16-x}]^{2-}$ species could be deduced.

Finally, the reaction of 8 equiv of isonicotinic acid with **1** was explored in an effort to prepare a new type of Mn_{12} cluster with dangling pyridine groups. The reaction led to the formation of a dark brown precipitate, but the product proved to be sufficiently soluble such that ESI-MS data could be obtained. ESI-MS data on the solution showed the presence of substitution products with the composition of trifluoroacetate−isonicotinate varying from 15:1 to 9:7. Further experiments are in progress to optimize the formation of a fully substituted product of the reaction.

(58) Details for the experimental for the reactivity studies and the corresponding data are submitted as Supporting Information.

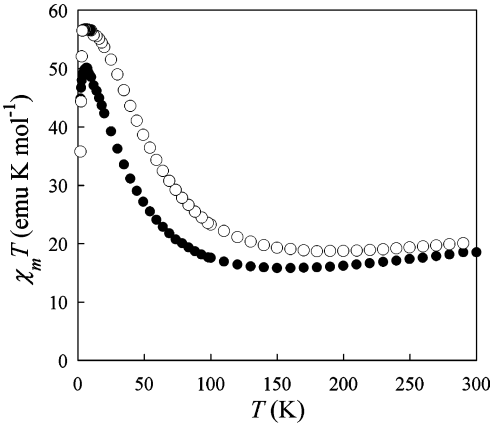

Figure 7. Thermal variation product ($\chi_m T$) versus temperature (T) for $[Mn_{12}O_{12}(CF_3COO)_{16}(H_2O)_4]\cdot 2CF_3COOH\cdot 4H_2O$ (**1**) (●) and $[Mn_{12}O_{12}(CF_3COO)_{16}(H_2O)_4]\cdot CF_3COOH\cdot 7H_2O$ (**2**) (○) in an applied dc field of 1000 G.

Magnetic Properties of Compounds 1 and 2. Magnetic susceptibility measurements were performed on crushed single crystals of $[Mn_{12}O_{12}(CF_3COO)_{16}(H_2O)_4]\cdot 2CF_3COOH\cdot 4H_2O$ (**1**) and $[Mn_{12}O_{12}(CF_3COO)_{16}(H_2O)_4]\cdot CF_3COOH\cdot 7H_2O$ (**2**) frozen in eicosane at 1000 G in the 1.8−300 K temperature range (Figure 7). The $\chi_m T$ product for **1** remains relatively constant at ∼18−20 emu K mol^{-1} in the 300−130 K range, which is lower than the theoretical value for noninteracting spins (31.5 emu K mol^{-1}). This behavior is an indication of antiferromagnetic coupling within the cluster. The $\chi_m T$ product passes through a minimum, before increasing rapidly to a maximum value of ∼55 emu K mol^{-1} at 3.5 K, followed by a sharp decrease down to 1.8 K. The observed maximum for the $\chi_m T$ product is indicative of the stabilization of a high-spin ground state, whereas the sharp decrease at low temperatures can be attributed to zero-field splitting (ZFS) effects. The $\chi_m T$ product for compound **2** varies from ∼16 to 19 emu K mol^{-1} over the 300−100 K temperature range. At temperatures below the minimum at 140 K, $\chi_m T$ increases to a maximum value of ∼50 emu K mol^{-1} at 6.5 K followed by a sharp decrease down to 2 K.

An examination of the ground states for **1** and **2** was carried out by fitting the magnetization (M) data using the program ANISOFIT.[59] Plots of M versus H/T for **1** and **2** from 1 to 7 T in the 1.8−4.0 K range are depicted in Figures 8 and 9, respectively. The best fitting for **1** was obtained with the parameters $S = 10$, $g = 2.15$, $D = -0.65$ cm^{-1}, and $E = 0$ cm^{-1}; compound **2** was best fit to $S = 10$, $g = 1.87$, $D = -0.34$ cm^{-1}, and $E = -0.10$ cm^{-1} (where D is the axial zero field splitting (ZFS) parameter and E is the rhombic ZFS parameter). The two complexes give rise to different fitting parameters, but the values fall within the range that is typical for Mn_{12} complexes. The magnetization data for **1** and **2** approach values of ∼18.6 μ_B (Figure 10) and ∼16.8 μ_B (Figure 11), respectively, but saturation was not observed. The magnetization measurements indicate that compound **1** displays the expected hysteresis loop at 2 K, whereas compound **2** does not. These observations are in accord with the presence of a lower barrier for magnetization

(59) Shores, M. P.; Sokol, J. J.; Long, J. R. *J. Am. Chem. Soc.* **2002**, *124*, 2279−2292.

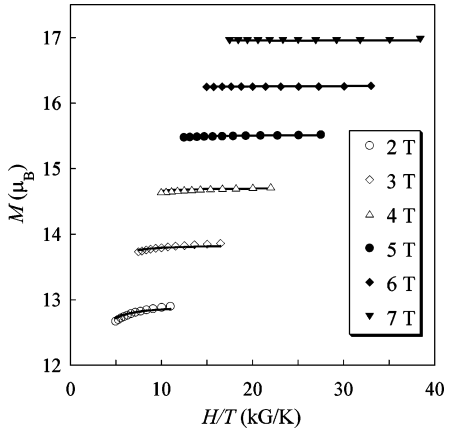

Figure 8. Plot of M vs H/T for compound **1** in the 0−7 T range from 1.8 to 4.0 K. The solid lines represent the best fit to the parameters $S = 10$, $g = 2.15$, $D = -0.65$ cm^{-1}, and $E = 0$ cm^{-1}.

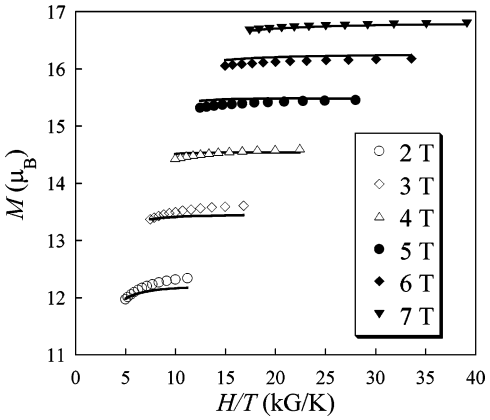

Figure 9. Plot of M vs H/T for compound **2** in the 0−7 T field range from 1.8 to 4.0 K. The solid lines represent the best fit to the parameters $S = 10$, $g = 1.87$, $D = -0.34$ cm^{-1}, and $E = -0.10$ cm^{-1}.

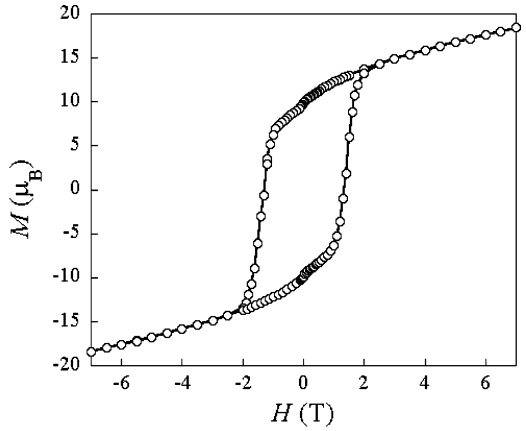

Figure 10. Field dependence of the magnetization for $[Mn_{12}O_{12}(CF_3COO)_{16}(H_2O)_4]\cdot 2CF_3COOH\cdot 4H_2O$ (**1**) at $T = 1.8$ K.

reorientation for **2**, as expected due to the much lower blocking temperature.

Alternating Current (Ac) Susceptibility Measurements. In a single-molecule magnet, a potential energy barrier, U, traps the magnetic moment in a spin "up" or spin "down" state. This thermal barrier is directly related to the total spin ground state (S) and the uniaxial anisotropy of the molecule and can be expressed by the relationship, $U = S^2|D|$, for an integer spin system (where D is the axial ZFS parameter of

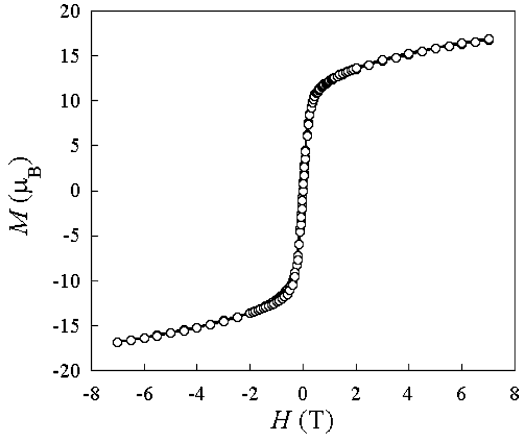

Figure 11. Field dependence of the magnetization for $[Mn_{12}O_{12}(CF_3COO)_{16}(H_2O)_4]\cdot CF_3COOH\cdot 7H_2O$ (**2**) at $T = 1.8$ K.

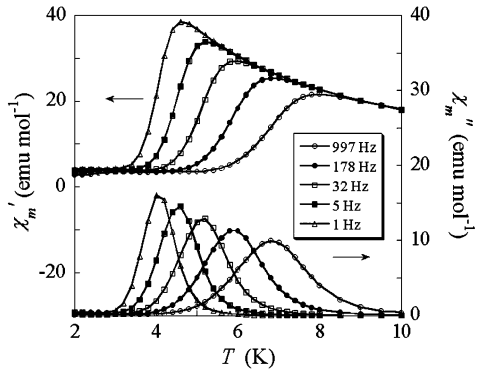

Figure 12. Plot of the in-phase (χ_m') and out-of-phase (χ_m'') ac magnetic susceptibility signals vs temperature (T) for $[Mn_{12}O_{12}(CF_3COO)_{16}(H_2O)_4]\cdot 2CF_3COOH\cdot 4H_2O$ (**1**).

the molecule). In an ac susceptibility experiment, a weak oscillating field is applied to a sample to probe the magnetic relaxation dynamics of the sample. When the operating frequency of the ac field is comparable to the rate at which the magnetic moment of the molecule reorients itself, an out-of-phase (χ_m'') ac susceptibility signal is observed. The signature of an SMM is a frequency-dependent χ_m'' signal, a feature that is used to extract the effective energy barrier for reorientation (U_{eff}).

The ac susceptibility measurements were performed on crushed crystals of compounds **1** and **2**. For compound **1**, the in-phase (χ_m') and out-of-phase (χ_m'') magnetic susceptibility data (Figure 12) adhere to the same behavior as the Mn_{12}-acetate complex, namely the appearance of a χ_m'' signal in the 4−7 K temperature range. For compound **2**, however, the frequency-dependent χ_m'' signal falls in the 2−4 K temperature range (Figure 13). The absence of a χ_m'' signal at $T > 4$ K (Figure 13, inset) demonstrates that compound **2** is pure and is not contaminated with quantities of compound **1**. The fact that the χ_m'' signal for compound **2** occurs at lower temperatures than compound **1** is an indication of a lower thermal barrier and/or different relaxation pathways.

The rate of magnetization relaxation ($1/\tau$) of a molecule corresponds to the peak maximum of the ac out-of-phase (χ_m'') signal, at which temperature it is equal to the frequency of the applied ac field. The frequency dependence of the

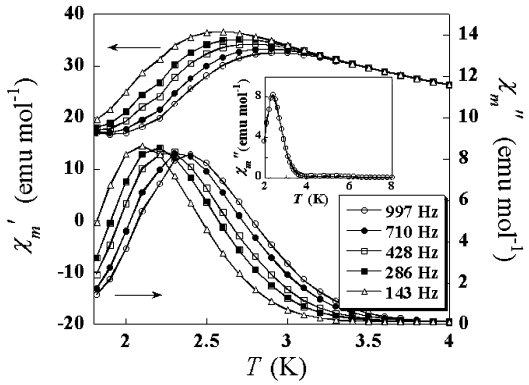

Figure 13. Plot of the in-phase (χ_m') and out-of-phase (χ_m'') ac magnetic susceptibility signals vs temperature (T) for $[Mn_{12}O_{12}(CF_3COO)_{16}(H_2O)_4]\cdot CF_3COOH\cdot 7H_2O$ (**2**). Inset: χ_m'' signal for **2** at 997 Hz in the 2−8 K temperature range.

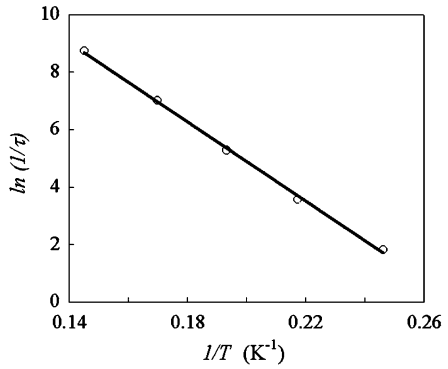

Figure 14. Plot of the natural logarithm of the rate of relaxation ($\ln(1/\tau)$) vs the inverse temperature ($1/T$) for $[Mn_{12}O_{12}(CF_3COO)_{16}(H_2O)_4]\cdot 2CF_3COOH\cdot 4H_2O$ (**1**). The solid line is a least-squares fit of the data; see text for fitting parameters.

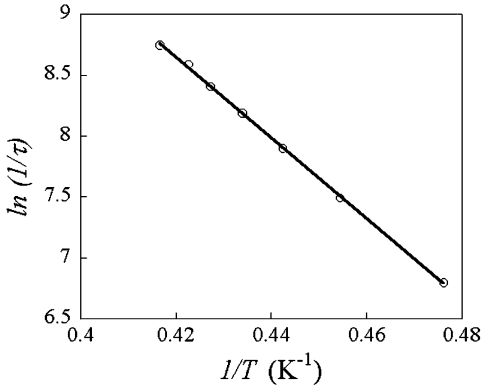

Figure 15. Plot of the natural logarithm of the rate of relaxation ($\ln(1/\tau)$) vs the inverse temperature ($1/T$) for $[Mn_{12}O_{12}(CF_3COO)_{16}(H_2O)_4]\cdot CF_3COOH\cdot 4H_2O$ (**2**). The solid line is a least-squares fit of the data; see text for fitting parameters.

χ_m'' signal can be used to plot $\ln(1/\tau)$ vs $1/T$ to determine the effective potential energy barrier (U_{eff}) for magnetization reorientation using the Arrhenius equation, $\ln(1/\tau) = -U_{eff}/kT + \ln(1/\tau_0)$ (where k is the Boltzmann constant and $1/\tau_0$ is the preexponential term). Plots of $\ln(1/\tau)$ vs $1/T$ for compounds **1** and **2** are depicted in Figures 14 and 15, respectively. A least-squares fitting of the data leads to $U_{eff} = 48$ cm^{-1} and $1/\tau_0 = 7.4 \times 10^{-9}$ s^{-1} for compound **1** and $U_{eff} = 15$ cm^{-1} and $1/\tau_0 = 1.6 \times 10^{-10}$ s^{-1} for compound **2**.

The different rates of magnetization relaxation for compounds **1** and **2** appear to be the direct result of the "Jahn−Teller isomerism", which refers to the orientation of the JT axes of the Mn^{III} ions in the Mn_{12} core. This phenomenon has been previously noted[25,33,45,47] and described in detail elsewhere.[3] Whereas the orientations of the elongated JT axes are all approximately perpendicular to the plane of the molecular core for compound **1**, there are different orientations of the JT axes in compound **2** that result in at least one elongated axis being canted toward the approximate equatorial plane. Since the total axial ZFS parameter (D) of the molecule is a vectorial projection of the single ion ZFS splitting parameters,[60] the arrangement of the elongated JT axes of the Mn(8) and Mn(12) atoms in compound **2** is expected to result in a smaller $|D|$ value, which leads to a lower thermal barrier (U). The fitting of the magnetization data supports this argument, as the magnitude of $|D|$ for **1** is approximately twice that of **2**. More importantly, the considerably lower site symmetry of the Mn atoms in compound **2** leads to a nonzero rhombic ZFS parameter ($E = -0.10$ cm^{-1}). This consequently increases the transverse interactions, an important factor for tunneling, leading to a lower effective energy barrier for reorientation. The same mechanism for tunneling is not operative in compound **1** due to the higher site symmetry and smaller rhombic ZFS interactions. It has been recently noted, however, that the degree of magnetic anisotropy for Mn_{12}-acetate is related to the presence of disordered acid of crystallization.[61] Unfortunately, the structural disorder of the triflouroacetatic acid of crystallization could not be resolved for compound **1** down to 30 K to confirm the precise site symmetry of the Mn centers. With the present data in hand, we can only state that compound **2** possesses *relatively* lower site symmetry than compound **1**.

Concluding Comments

This study has demonstrated that it is possible to fully substitute the acetate ligands in $[Mn_{12}O_{12}(CH_3COO)_{16}(H_2O)_4]$ (Mn_{12}-acetate) with triflouroacetate groups to yield two isomeric forms of the product. The treatment of Mn_{12}-acetate with CH_2Cl_2/CF_3COOH and/or neat CF_3COOH afforded two isomers of the new single-molecule magnets, $[Mn_{12}O_{12}(CF_3COO)_{16}(H_2O)_4]\cdot 2CF_3COOH\cdot 4H_2O$ (**1**) and $[Mn_{12}O_{12}(CF_3COO)_{16}(H_2O)_4]\cdot CF_3COOH\cdot 7H_2O$ (**2**), respectively. Interestingly, it was found that one can preferentially favor the isolation of only one of the JT isomers in a pure form by the use of certain reaction conditions. A mixture of organic solvent and CF_3COOH leads to crystals of isomer **1**, whereas the use of neat CF_3COOH leads to the isolation of solely isomer **2**. ESI-MS techniques proved to be a successful method for monitoring the course of the reaction and for detecting samples that represent incomplete substitution. Compound **1** exhibits a structural core that is nearly identical with that of the Mn_{12}-acetate starting material as well as

(60) HartmannBoutron, F.; Politi, P.; Villain, J. *Int. J. Mod. Phys. B* **1996**, *10*, 2577−2637.
(61) Cornia, A.; Sessoli, R.; Sorace, L.; Gatteschi, D.; Barra, A. L.; Daiguebonne, C. *Phys. Rev. Lett.* **2002**, *89*, 257201.

similar magnetic properties. On the other hand, compound **2** displays a considerably lower thermal barrier for magnetic relaxation as compared to **1** due to the lower site symmetry of the Mn^{III} ions and the canted orientation of two of the Jahn−Teller axes. An important outcome of this study is that three methods of characterization were required to support our claims that the bulk products are pure; these are single-crystal X-ray diffraction studies to determine the different structural motifs of the two compounds, ESI-MS to rule out contamination of the sample with acetate ligands, and magnetochemistry to confirm that the sample contains only one of the JT isomers. These issues of purity were particularly important in this study, as we were replacing the acetate ligand with the weaker base trifluoroacetate. A future goal of this study is to take advantage of the increased solubility of the clusters as well as the high lability of the $[CF_3CO_2]^-$ ligands in reactions to form clusters of higher nuclearity under mild conditions. The lower volatility of trifluoroacetate compounds versus acetate derivatives should also prove to be useful in experiments aimed at producing films of these molecules under mild conditions.

Acknowledgment. We thank the National Science Foundation for PI and NIRT grants (CHE-9906583 and DMR-0103455) and for equipment grants for the CCD X-ray equipment (CHE-9807975) and the SQUID magnetometer (NSF-9974899). Support from the Welch Foundation and from a Telecommunications and Informatics Task Force (TITF) Grant from Texas A&M University is also gratefully acknowledged.

Supporting Information Available: Crystallographic data in CIF format (**1** and **2**), listings of the TGA data (**1**, **2**, Mn_{12}-acetate), ESI-MS spectra (**2**, Mn_{12}-acetate), details of the magnetic measurements, and the results from the reactivity studies for **1**. This material is available free of charge via the Internet at http://pubs.acs.org.

IC030144P